RSC Advances

PAPER

View Article Online
View Journal | View Issue

Cite this: *RSC Adv.*, 2024, **14**, 15240

Preparation and characterization of polydopamine and *n*-butyl methacrylate copolymer coatings on titanium–nickel alloy stents

Yuanhui Liu,[a] Guocheng Jin,[b] Han Miao[a] and Shiai Xu *[ac]

Cardiovascular diseases pose a significant global health threat, and stents play a crucial role in managing these diseases. However, challenges exist with respect to the poor adhesion of stent coatings. Cardiac stents are often composed of titanium–nickel (TiNi) alloys as the metallic component and poly(*n*-butyl methacrylate) (PBMA) as the coating. The poor adhesion of PBMA to TiNi alloy surface may cause detachment and subsequent thrombosis post-implantation. This study utilizes Reversible Addition-Fragmentation Chain Transfer (RAFT) polymerization to synthesize a novel block copolymer, PBMA-*b*-PVP, composed of PBMA and poly(*N*-vinylpyrrolidone) (PVP). TiNi alloy surfaces are functionalized with polydopamine (PDA) to enhance polymer coating adhesion. PBMA-*b*-PVP exhibits a remarkable improvement in adhesion from class 5 to class 0 and high coating stability after a 15 days immersion in a phosphate buffer solution. The corrosion current density is reduced by 44% with the incorporation of PDA into PBMA-*b*-PVP coatings, suggesting high corrosion resistance. PDA-functionalized coatings promote cell viability without cytotoxicity, suggesting high biocompatibility. This study provides a robust strategy for preparing stent coatings with high adhesion, corrosion resistance, and biocompatibility.

Received 26th February 2024
Accepted 6th May 2024

DOI: 10.1039/d4ra01491j

rsc.li/rsc-advances

1 Introduction

Cardiovascular diseases are at the forefront of global health concerns[1] and are among the top 10 causes of mortality worldwide according to the World Health Organization.[2] In clinical practice, stents made of materials such as stainless steel, cobalt–chromium alloy, or tantalum are prevalent for managing cardiovascular diseases.[3] However, the inherent limitations of these materials, such as low elastic resilience, may undermine the performance and long-term stability of stents. In recent years, titanium–nickel (TiNi) alloy stents have received considerable attention because their remarkable biocompatibility and the effect of shape memory can alleviate patient discomfort and postoperative complications.[4] However, in-stent restenosis remains a significant problem primarily due to the proliferation and migration of vascular smooth muscle cells within bare metal stents. A promising solution to this problem is to use drug-eluting stents (DES) in which a drug-coated layer is incorporated on the metal surface with compounds like paclitaxel and rapamycin to inhibit endothelial cell proliferation. The polymer coating is a crucial component of DES,[5,6] because it serves as an adhesive layer between the drug layer and the metal layer and enhances biocompatibility, isolates the metal from the vessel wall, and reduces metal ion release.[7] A variety of polymers, including polyethylene, polystyrene, polyacrylic acid, methacrylate,[8] block copolymers[9] and blends,[10] have been employed for stent coatings. Among these, poly(*n*-butyl methacrylate) (PBMA) has emerged as a favorable choice due to its high biocompatibility and stability,[11] and the minimal platelet adsorption and activation help to prevent tissue irritation and allergic reactions.[12] However, the adhesion between PBMA and metal surface may not be high enough to withstand shear and dilatation forces in the vessel, potentially leading to coating cracking and peeling.[13]

The durability of DES *in vivo* critically depends on the adhesion of the coating. Polyvinylpyrrolidone (PVP), a polar polymer with carbonyl groups and pyrrolidone ring is commonly employed in various applications such as drug delivery,[14] anti-fouling coatings,[15] wound adhesives,[16] wound dressings, and disinfectants.[17] However, few studies have been done on stent coating. PVP holds promise in facilitating adhesion to metal surfaces.[18,19] However, the low water solubility of PVP may limit its applicability in stent coatings when exposed to blood.[20] To address this challenge, we developed a new approach for synthesizing an amphiphilic and water-insoluble block copolymer, poly(*n*-butyl methacrylate)-*b*-poly(*N*-vinylpyrrolidone) (PBMA-*b*-PVP), through Reversible Addition-Fragmentation Chain Transfer polymerization (RAFT). This method enables precise control over the polymeric structure and molecular weight,[21] and the utilization of a block copolymer

[a]*School of Materials Science and Engineering, East China University of Science and Technology, Shanghai 200237, China. E-mail: saxu@ecust.edu.cn*
[b]*Shanghai Flowridge Material Technology Co., Ltd, Shanghai 201318, China*
[c]*Qinghai Provincial Key Laboratory of Salt Lake Materials Chemical Engineering, School of Chemical Engineering, Qinghai University, Xining 810016, China*

eliminates potential microphase separation and the resultant coating non-uniformity and instability in properties that may arise from the simple physical mixture of two homopolymers.

Polydopamine (PDA) acts as a versatile load-transfer bridge to enhance metallic surfaces. PDA is commonly employed for surface modification of various material matrices, including metals,[22] organic materials,[23] and inorganic materials.[24] A unique characteristic of PDA is its gentle adhesion to various materials, and therefore polymer–metal junctions are strengthened through interactions with other polymers.[22,25,26]

In this study, the block copolymer PBMA-*b*-PVP consisting of PBMA and four different chain lengths of PVP was synthesized by RAFT polymerization, and functionalized TiNi alloys with PDA. The effect of the adhesion of PBMA-*b*-PVP with different PVP chain lengths to the surfaces of TiNi alloys was investigated, as well as the stability of the PBMA-*b*-PVP in PBS solution. The impact of PDA-functionalized TiNi alloy on the adhesion of polymeric coatings and its effects on the corrosion resistance and biocompatibility of the TiNi alloy were also investigated.

2 Experiments

2.1 Materials

TiNi alloy was purchased from Guangyuan Metal Materials Co. Ltd (Suzhou, China). Butyl methacrylate (≥99%) and vinyl pyrrolidone (≥90%) were purchased from Titan Science Co., Ltd (Shanghai, China). Butyl methacrylate and vinyl pyrrolidone were purified by distillation under reduced pressure to remove inhibitors and water before use. Toluene, trichloromethane, petroleum ether, and methanol were purchased from Aladdin Reagent Co., Ltd (Shanghai, China). Diisopropyl xanthate disulfide (≥98.0%) was purchased from Yuanye Biotechnology Co., Ltd (Shanghai, China). PBS was purchased from Hongcang Biotechnology Co., Ltd (Fuzhou, China).

2.2 Synthesis and characterization of PBMA-*b*-PVP

PBMA-*b*-PVP was synthesized by RAFT polymerization using diisopropyl xanthate disulfide (DIP) as the chain transfer agent[27,28] by two-step polymerization. In the first step, BMA (14.200 g, 100 mmol), 2,2-azobisisobutyronitrile (AIBN) (0.138 g, 0.8 mmol), DIP (0.149 g, 0.66 mmol) and toluene (10 mL) were added to a Schlenk flask under magnetic stirring and then reacted under a nitrogen atmosphere at 68 °C for 1.5 h. The reaction solution was diluted with toluene and added dropwise into a large volume of ice-cold methanol under stirring, and then isolated by filtration and washed with methanol. After drying, the crude product was redissolved in toluene and precipitated again in methanol. This purification step was repeated for three times. The product of PBMA was thoroughly dried in a vacuum oven at 40 °C for 24 h.

In the second step, the as-synthesized initial block PBMA, which also served as the macromolecular RAFT agent, was utilized in the subsequent synthesis of the PVP block. Four batches of PBMA-*b*-PVP with different lengths of PVP block were synthesized and denoted as PBMA-*b*-PVP-1, PBMA-*b*-PVP-2, PBMA-*b*-PVP-3, and PBMA-*b*-PVP-4, respectively. In the detailed experimental procedure, PBMA (1.501 g, 0.06 mmol) samples were dissolved in 10 mL of toluene under magnetic stirring. Then *N*-vinylpyrrolidone (1.199 g, 10.80 mmol) and AIBN (0.050 g, 0.291 μmol) were added into the solution. The reactions were conducted under nitrogen atmosphere at 68 °C for 3 h, 4 h, 5 h and 6 h, respectively, and terminated by rapid cooling. The products were diluted in toluene and precipitated into petroleum ether[28] for purification. Purification was repeated for three times and the final products were thoroughly dried in vacuum.

The resulting block copolymers were characterized to elucidate their structural properties and ensure the success of the synthetic processes. Fourier transform infrared spectroscopy (FTIR) was carried out with a Nicolet 6700 spectrometer. The nuclear magnetic resonance (^{1}H NMR) spectra of the copolymers were captured on a Bruker Fourier 400 MHz spectrometer using chloroform-d ($CDCl_3$) as the solvent. And the molecular weights and polydispersity index (PDI) of PBMA and PBMA-*b*-PVP were determined by gel permeation chromatography (GPC) using WATERS 1515 with THF as the eluent.

2.3 PDA-functionalization of TiNi alloy sheets

TiNi alloy sheets were polished with 600, 800, and 1000 grit SiC paper, cleaned with acetone and ethanol for 20 min, and then dried at 40 °C. After that, the sheets were immersed in a solution containing 10 mM Tris(hydroxymethyl) aminomethane, and the pH was adjusted to 8.5 using hydrochloric acid. The solution was further supplemented with 3.0 g L^{-1} dopamine. The TiNi alloy sheets were immersed in this solution for 24 h and then rinsed with deionized water.[28] Finally, the sheets were dried at 50 °C for 4 h.

2.4 Surface characterization of TiNi alloy sheets

The surface morphologies of the TiNi alloy sheets before and after modification, were observed using an S-4800 field-emission scanning electron microscope (SEM, Hitachi). The elemental compositions were determined by X-ray photoelectron spectroscopy (XPS) using a Thermo Scientific K-Alpha+ with an Al Kα as the source operated at 12 kV voltage and 6 mA current.

2.5 Adhesion tests of coatings

To evaluate the adhesion strength of the coatings, a cross-cut test was conducted in accordance with ISO 2409 : 2013 standards.[29] A solution containing 1% polymer in acetone as the solvent was prepared. Subsequently, 625 μL of the solution was uniformly sprayed over a 2.5 cm × 2.5 cm area using a spray gun. Scratch tests were performed on the composite films using a cutting blade with 11 teeth spaced 1.0 mm apart. The procedure created a cross-shaped pattern on the coating at a 90° angle. Following this, adhesive tape was applied to the coated surface and removed after 90 seconds of adherence. The coating was then examined to assess the degree of breakage, and the extent of peeling was graded on a scale from 0 to 5 to quantify the bond strength. In this grading system, the adhesion strength decreases from grade 0 to grade 5.

2.6 Surface morphologies of coatings under wet conditions

The coatings with PDA-TiNi as the metal substrate are prepared as described in Section 2.5 and subsequently transferred to individual 50 mL centrifuge tubes filled with PBS solution. The tubes were incubated at 37 °C in a shaker at 100 rpm for 15 days. After that, the surface morphologies of the coatings were examined by SEM.

2.7 Electrochemical corrosion tests

Electrochemical corrosion tests were conducted using a conventional three-electrode system on the electrochemical workstation (PARSTAT2273). An inert platinum electrode and a saturated potassium chloride reference electrode were incorporated into the setup. The testing system was immersed in a water bath at 37 °C, and the PBS solutions was used to simulate the body fluid. The potential polarization curve was obtained at a scanning rate of 5 mV s^{-1} within a scan range from −0.6 V to 1.5 V.[30]

2.8 Cytotoxicity tests

To assess the biocompatibility of different coatings, cytotoxicity tests were conducted. Sample preparation involved the use of Minimum Eagle's Medium (MEM), and each sample was incubated at 37 °C for 24 h to collect leachate. Simultaneously, L929 cells were calibrated to a density of 10 000 cells per milliliter and then inoculated into the wells of a 96-well plate. They were further incubated for an additional 72 h. The culture medium in each well was carefully replaced with 100 μL of the prepared leachate. Subsequently, 50 μL of the Cell Counting Kit-8 (CCK-8) solution was introduced to each well, followed by further incubation for 2 h. Cell viability was assessed by precisely measuring the absorbance at a wavelength of 450 nm using a microplate reader.[30]

3 Results and discussion

3.1 Synthesis of PBMA-*b*-PVP

^{1}H NMR, FTIR spectroscopy and GPC were utilized to investigate the chemical structure, weight-average molecular weights (M_w), number-average molecular weights (M_n) and polydispersity index (PDI) of the products. The ^{1}H NMR and FTIR results of synthesized copolymers with different PVP chain lengths are shown in Fig. 1. In Fig. 1a, the characteristic peaks of the methyl and methylene groups in the PBMA chain are observed at $\delta = 0.88$–1.04 ppm and 1.42 ppm, respectively.[31] The presence of the PVP chain is confirmed by the peaks of methylene close to nitrogen in a five-membered ring at approximately $\delta = 3.23$ ppm. The characteristic peak of the hypomethyl group in the PVP chain is observed at 3.74 ppm.[32] These results indicate that PBMA-*b*-PVP is successfully synthesized.

In Fig. 1b, the distinctive peak at 1730 cm^{-1} is due to the stretching vibration of carbonyl (–O–C=O–), while that at 1650 cm^{-1} is due to the stretching vibration of carbonyl (N–C=O) in PBMA-*b*-PVP,[33] and its intensity increases proportionally with the PVP content.

Table 1 provides the weight-average molecular weights (M_w), number-average molecular weights (M_n), and PDI for PBMA and

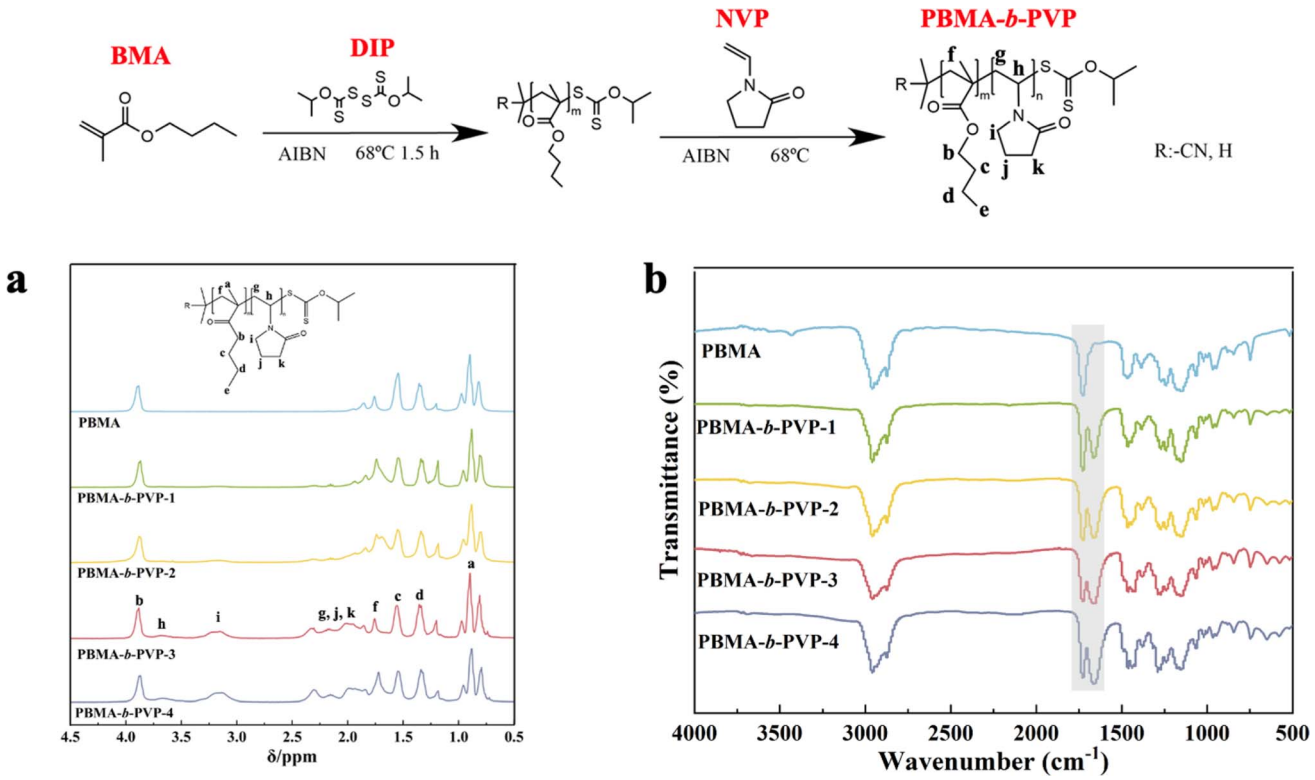

Fig. 1 ^{1}H NMR (a) and FTIR (b) spectra of synthesized copolymers with different PVP chain lengths.

Table 1 Molecular weights and distributions of PBMA and copolymers with different PVP chain lengths

Items	M_n	M_w	PDI
PBMA	25 027	43 735	1.74
PBMA-*b*-PVP-1	31 122	48 305	1.55
PBMA-*b*-PVP-2	34 231	54 534	1.59
PBMA-*b*-PVP-3	41 810	55 686	1.33
PBMA-*b*-PVP-4	43 529	56 166	1.29

PBMA-*b*-PVP. It is demonstrated that the molecular weight of PBMA-*b*-PVP-1 to PBMA-*b*-PVP-4 becomes larger and the PDI decreases, which is consistent with RAFT polymerization. Four copolymers with different PVP chain lengths were successfully synthesized as confirmed by ^{1}H NMR, FTIR spectroscopy and GPC results.

3.2 Surface characteristics of TiNi alloy sheets

Fig. 2 shows the microstructures of untreated TiNi alloy (TiNi) and PDA-functionalized TiNi alloy (PDA-TiNi) at different magnifications. Fig. 2a and b illustrate that TiNi has a smooth surface with some regular scratches and rolling lines resulting from the processing of the TiNi alloy. Fig. 2c reveals that PDA-TiNi has a layer of spherical particles of different sizes on the surface, this non-homogeneous deposition phenomenon is attributed to the uneven adsorption of PDA molecules on the surface.[34] Fig. 2d indicates the formation of spherical PDA particles on the surface, suggesting that dopamine undergoes spontaneous oxidation and polymerization on the substrate surface to form PDA.[35]

The elemental compositions and valence states of the TiNi and PDA-TiNi surfaces were investigated by XPS to demonstrate the successful functionalization of TiNi alloys by polydopamine. Fig. 3a–c display the XPS spectra of C 1s, N 1s, and O 1s of PDA-TiNi, respectively. In Fig. 3a, the peak observed at 284.6 eV is attributed to carbon oxides resulting from air impurities. The peaks at 286.0 and 287.2 eV are attributed to carbon present in C–OH and CH_2–NH_2 groups in PDA. The N 1s spectrum is fitted with three peaks corresponding to tertiary amine (R–N, at 398.4 eV), secondary amine (R–NH, 399.7 eV), and primary amine (R–NH_2, 401.4 eV), respectively.[36] The O 1s spectrum is also fitted with three peaks corresponding to TiO_2 (530.6 eV), C=O (532.2 eV), and O–H (532.8 eV), respectively,[37] indicating the formation of a PDA coating on the substrate surface. Dopamine undergoes polymerization through oxidation, leading to the formation of intermediates and tautomeric forms. According to the chemical structures of PDA, possible intermediates and their structures can be inferred as follows. R–NH_2 is derived from PDA, R_2–NH is associated with both intermediate species and PDA, and R–N= is associated with tautomeric species of the intermediate species 5,6-dihydroxyindole and 5,6-indolequinone.[36] Fig. 3d displays the XPS spectra of TiNi and PDA-TiNi, and their elemental compositions are listed in Table 2. PDA functionalization results in an increase in the intensity of the N 1s peak but a decrease in the intensity of the Ti 2p peak. The atomic percentage of N 1s in PDA-TiNi is increased from 2.23% to 6.16%, indicating successful PDA functionalization on the surface of the TiNi alloy. The Ti content is significantly decreased from 10.31% to 0.67%, which is primarily due to the higher susceptibility of Ti to oxidation compared to Ni and subsequent accumulation of TiO_2 on the alloy surface.[38] The catechol group in PDA forms robust coordination complexes with TiO_2 on the TiNi alloy surfaces, leading to a substantial reduction in Ti content.[39] On the surface of TiNi, aside from the presence of C and O as inherent surface constituents, trace amounts of nitrogen (up to approximately 2.23) have been detected. Additionally, occasional observation of other elements suggests that these impurities stem from the lubricants and processing equipment employed during manufacturing.[40]

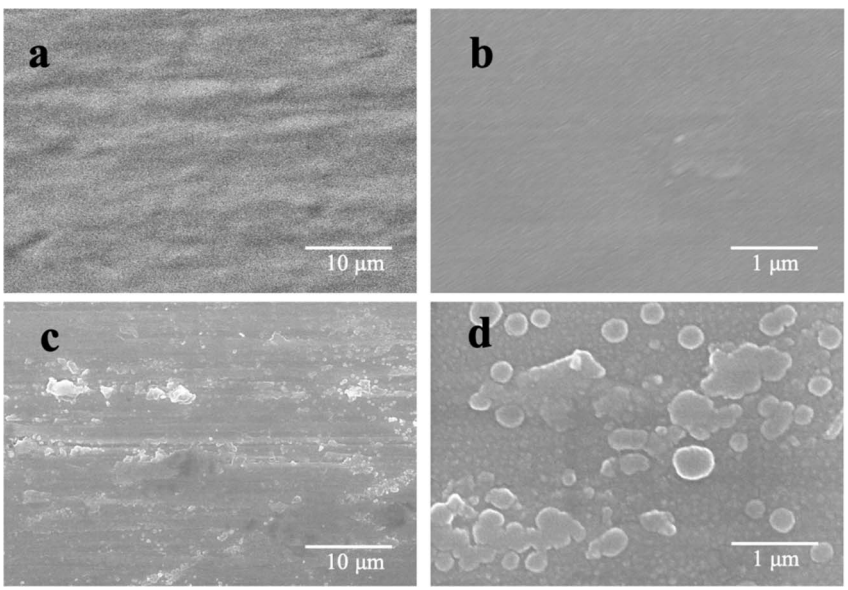

Fig. 2 SEM images of (a and b) TiNi and (c and d) PDA-TiNi.

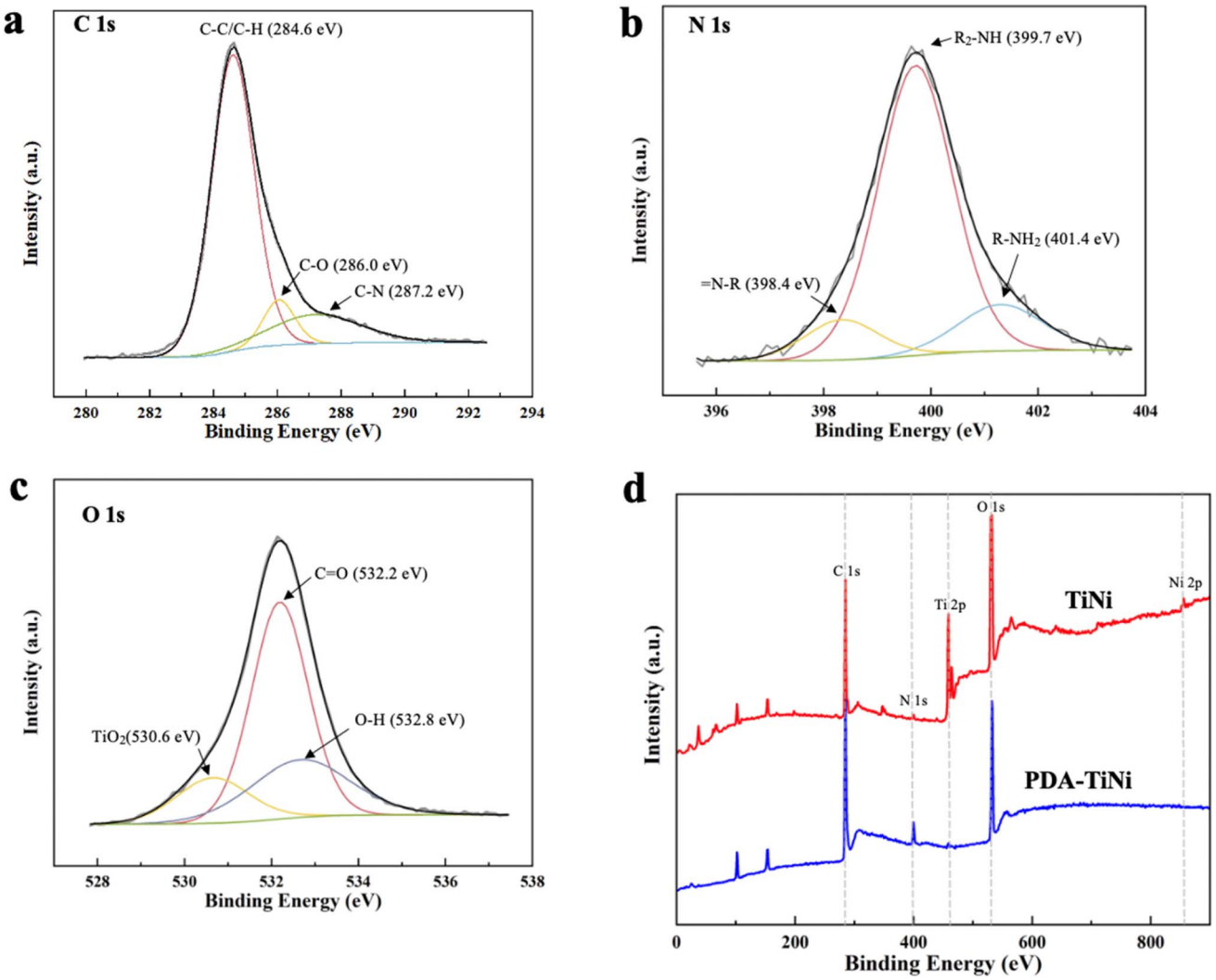

Fig. 3 C 1s (a), N 1s (b) and O 1s (c) peak-fitting curves of PDA-TiNi and (d) XPS spectra of degreased TiNi and PDA-TiNi.

Table 2 Surface elemental compositions of TiNi and PDA-TiNi

Atomic% specimen	Ti	Ni	O	C	N
TiNi	10.31	1.18	38.84	46.78	2.23
PDA-TiNi	0.67	0.44	24.32	68.41	6.16

3.3 The effects of PBMA/PVP ratio on adhesion

Cross-cut tests were performed to investigate the adhesion strength of different coatings. Grade 0 incisions are smooth and taped without breakage, while grade 5 indicates a large area of detachment. The cross-cut tests reveal that the PBMA coating exhibits significant peeling with a tape adhesion level of 5. Interestingly, as the PVP chain length increases, the adhesion properties show an initial improvement followed by deterioration. The adhesion levels of PBMA-*b*-PVP-1 to PBMA-*b*-PVP-4 are 1, 0, 0, and 2, respectively. The adhesion level of PBMA is 3 after the deposition of PDA on the surface of the TiNi alloy, while that of PBMA-*b*-PVP-1 to PBMA-*b*-PVP-3 coatings are consistently rated as level 0, and PBMA-*b*-PVP-4 coatings have an adhesion level of 1.

The adhesion strength between the coating and substrate is determined by molecular interactions at the interface. The enhanced adhesion is primarily attributed to the length of the PVP chain segments in PBMA-*b*-PVP. Increasing the number of polar groups can increase the interfacial interactions and ultimately the adhesion of the polymer coatings.[41] The enhanced adhesion of PVP chain segments on the TiNi alloy surfaces is attributed to the formation of coordination bonds between the nitrogen atoms in PVP and the active metal surface sites. This is facilitated by the elevated surface energy of PVP, which can promote the coverage of the metal surfaces.[19] However, the flexibility of PVP is lower than that of PBMA, and when the chain segments in PVP are too long, they are likely to tangle and fail to fully adapt to the shape of the TiNi alloy when in contact with the alloy, thus leading to a small contact area. A more rigid polymer has a lower deformation capacity when subjected to force, also making it difficult to fully adapt to the contact

surface. As a result, the mobility of chain segments is limited and the adhesion is adversely affected.[42]

The enhanced adhesion of PDA-TiNi compared to TiNi is attributed to the phenolic hydroxyl and amino groups in PDA, which can form hydrogen bonds and other interactive forces with the nitrogen-containing pyrrole ring and ester groups in the synthesized copolymer PBMA-*b*-PVP.[43,44] Consequently, PDA serves as an effective adhesion-promoting layer at the organic–inorganic interface.[26] The presence of PDA on TiNi surface increases the concentration of polar groups, thereby enhancing the metal surface wettability. The hydroxyl group in PDA facilitates the formation of additional hydrogen bonds with oxygen and nitrogen atoms in PBMA-*b*-PVP,[45] leading to improved wettability of the metal surface and consequently, a larger contact area between the coating and substrate.[46] This in turn significantly increases the spreading and bonding and ultimately the overall adhesion performance. In conclusion, the use of block copolymers and functionalizing the TiNi alloy with PDA could enhance the adhesion between PBMA and TiNi alloy surface (Fig. 4 and Table 3).

3.4 Surface morphology of coatings under wet conditions

The stability of the coating can be demonstrated by observing the surface morphology under wet conditions. Fig. 5 shows that after immersion in PBS for 15 days, the coatings of PBMA-*b*-PVP-1 and PBMA-*b*-PVP-2 remain largely intact, while some minor dissolution holes are present on the surface of PBMA-*b*-PVP-3 and PBMA-*b*-PVP-4. The high durability of PBMA-*b*-PVP-1 and PBMA-*b*-PVP-2 coatings can be attributed to their short PVP chains and the superior flexibility properties of the PBMA chains.[47] Due to its pronounced polarity, PVP demonstrates a notable affinity for interaction with water molecules. Surface-bound or superficial PVP chain segments tend to solubilize, while PVP chains embedded within the membrane are less soluble and more resistant to elution.[48] However, longer PVP chain segments become more polarized, as a consequence the interaction between water molecules and polymer chains is also increased.[49] The increased solubility of PVP facilitates the penetration of water into polymer coating, especially when they form a porous structure, and thus leads to accelerated dissolution of the coating.[50] To ensure that the coatings have good adhesion and remain stable, PBMA-*b*-PVP-2 was chosen as the coating based on the results of surface adhesion and morphology of PBMA-*b*-PVP-2 under wet condition.

3.5 Electrochemical corrosion performance

The potentiodynamic polarization curves of TiNi alloys subjected to different treatments, including PDA functionalization,

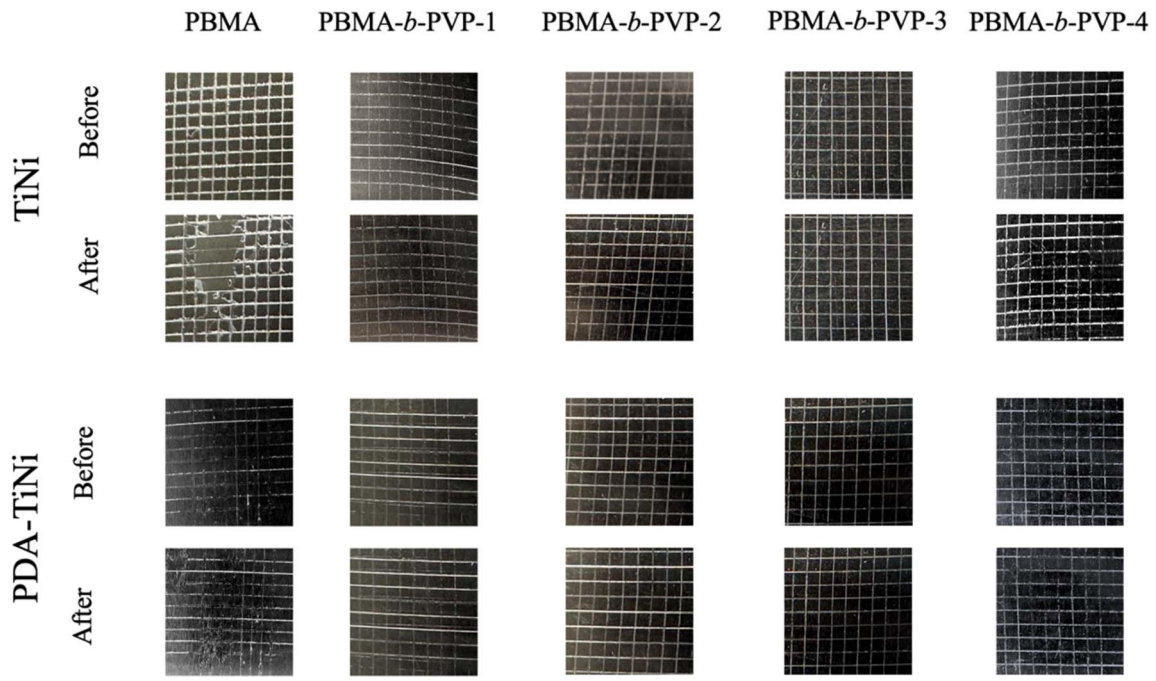

Fig. 4 Digital photographs of different coatings before and after cross-cut tests.

Table 3 Qualitative assessment of adhesion by cross-cut tests and optical image analysis

	PBMA	PBMA-*b*-PVP-1	PBMA-*b*-PVP-2	PBMA-*b*-PVP-3	PBMA-*b*-PVP-4
TiNi	5	1	0	0	2
PDA-TiNi	3	0	0	0	1

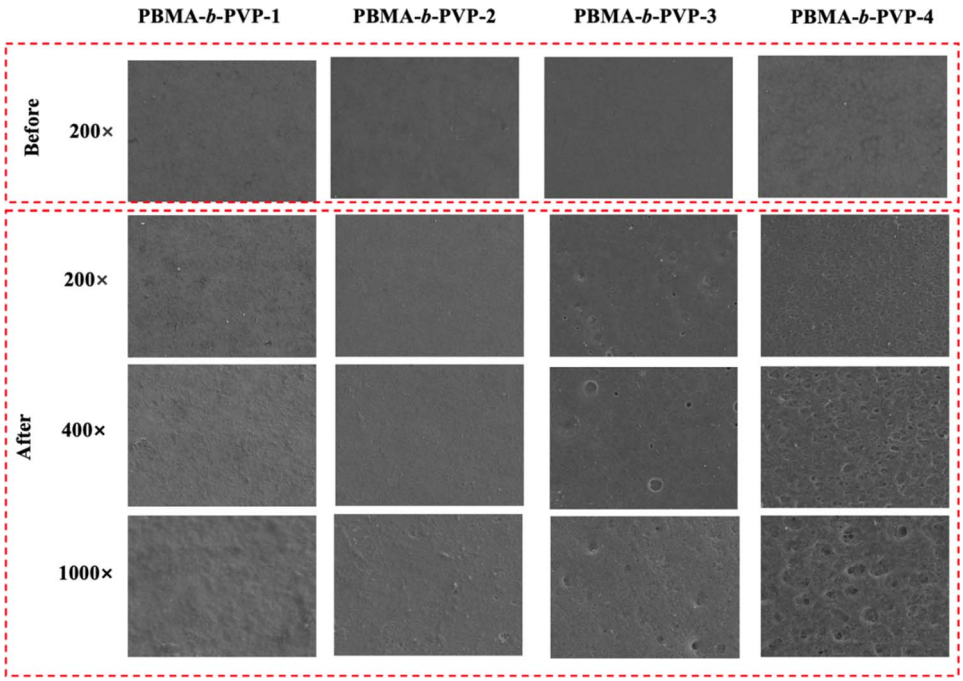

Fig. 5 SEM of PBMA-b-PVP-1, PBMA-*b*-PVP-2, PBMA-*b*-PVP-3, and PBMA-*b*-PVP-4 before and after 15 days immersion in PBS.

PBMA-*b*-PVP-2 coating (PBMA-*b*-PVP-2-TiNi), and a composite coating of PDA and PBMA-*b*-PVP-2 (PDA/PBMA-*b*-PVP-2-TiNi) in PBS, are shown in Fig. 6. The electrochemical parameters, corrosion potential (E_{corr}) and corrosion current density (I_{corr}) calculated from Tafel polarization curves are shown in Table 4. The lower I_{corr} values indicate a reduced corrosion rate of the material.[51] Compared to untreated TiNi, there is a significant increase in corrosion potential for PDA-TiNi and PBMA-*b*-PVP-2-TiNi, indicating high resistance to electrochemical corrosion.[52,53] These findings suggest a reduction in I_{corr} of about 44% compared to PBMA-*b*-PVP alone, demonstrating that PDA-functionalized composite coatings improve electrochemical corrosion resistance. This is because dopamine membranes are tightly bonded to the metal surface to effectively isolate the metal from contact with PBS.[54]

Table 4 Corrosion potential and corrosion current density of untreated and TiNi alloys of PDA-functionalized TiNi alloys

	E_{corr}, V	I_{corr}, A cm^{-2}
TiNi	−0.4859	1.5442×10^{-5}
PBMA-*b*-PVP-2-TiNi	0.0355	1.1158×10^{-6}
PDA-TiNi	−0.0181	8.9186×10^{-7}
PDA/PBMA-*b*-PVP-2-TiNi	0.0844	6.1432×10^{-7}

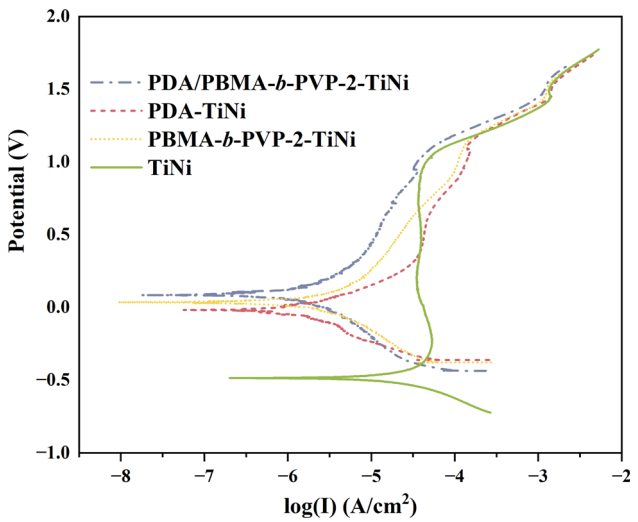

Fig. 6 Potentiodynamic polarization curves of PDA/PBMA-*b*-PVP-2-TiNi, PDA-TiNi, PBMA-*b*-PVP-2-TiNi and TiNi in PBS.

3.6 Cytotoxicity

In order to further compare the biocompatibility of TiNi, PBMA-*b*-PVP-2-TiNi, PDA-TiNi, PDA/PBMA-*b*-PVP-2-TiNi coatings, cytotoxicity experiments were conducted according to the standard ASTM 16886-5:2017.[55] The cytotoxic effects on the L929 cell line were evaluated by the Cell Counting Kit-8 assay. The results for all experimental groups are normalized against control cells. As shown in Fig. 7, after co-culture for 72 h, the relative cell accretion rate of the untreated TiNi alloy is 110.94, while the cell proliferation rates of the TiNi alloys coated with PBMA-*b*-PVP-2-TiNi, PDA-TiNi, and PDA/PBMA-*b*-PVP-2-TiNi are 119.93, 115.73, and 124.28, respectively. The cell proliferation rates for all samples exceeded 110%, indicating robust and healthy cell growth.[30] In conclusion, the surface of NiTi alloy modified by PDA and PBMA-*b*-PVP-2 shows no cytotoxicity and good biosafety.

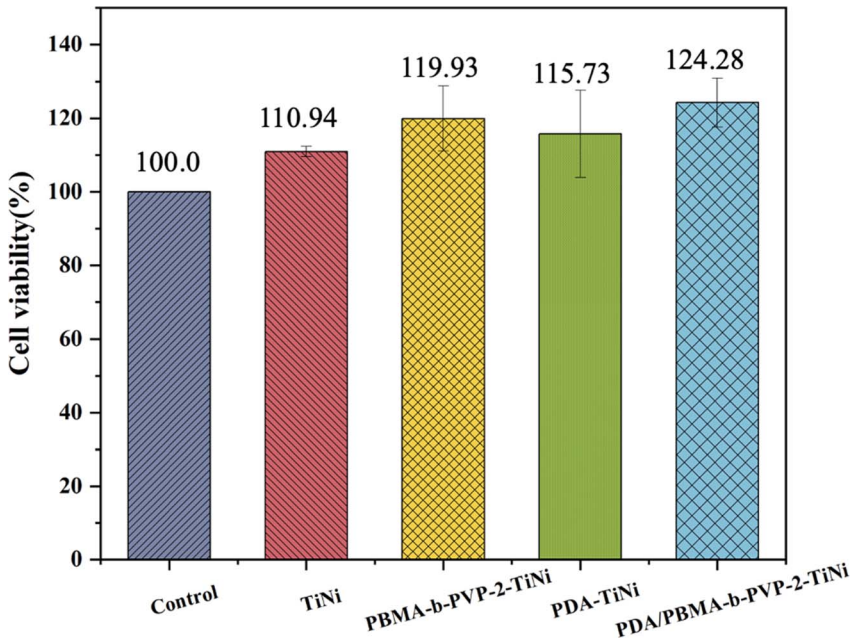

Fig. 7 Cytotoxicity of TiNi, PBMA-*b*-PVP-2-TiNi, PDA-TiNi, PDA/PBMA-*b*-PVP-2-TiNi coatings.

4 Conclusions

In this study, PBMA-*b*-PVP copolymers with different lengths of PVP chains are successfully synthesized by RAFT polymerization, and the influences of the composite coatings consisting of PBMA-*b*-PVP and PDA on the adhesion under dry and wet conditions, corrosion resistance, and biocompatibility of stents are investigated. Incorporation of PBMA copolymers with PVP blocks significantly enhances the adhesion to the stent surface, and functionalization of TiNi alloy with PDA further improves the adhesion of the polymer coating to TiNi alloy. The PBMA-*b*-PVP-2 coating is highly stable during 15 days immersion in PBS. The Tafel curves reveal significant reduction in corrosion, with PDA/PBMA-*b*-PVP-2-TiNi outperforming TiNi and PDA-TiNi. The cell proliferation rate is higher than 110%. This research provides an effective strategy to prepare stent coatings.

Conflicts of interest

There are no conflicts to declare.

Acknowledgements

This research is financially supported by the Shanghai Flowridge Material Technology Co. Ltd, the Young Scientists Fund of the National Natural Science Foundation of China (Grant No. 52203258), and Shanghai Pujiang Program (Grant No. 21PJ1402100).

References

1 J. E. Sousa, P. W. Serruys and M. A. Costa, *Circulation*, 2003, **107**, 2274–2279.
2 M. J. Friedrich, *JAMA, J. Am. Med. Assoc.*, 2019, **321**, 1041.
3 G. Mani, M. D. Feldman, D. Patel and C. M. Agrawal, *Biomaterials*, 2007, **28**, 1689–1710.
4 E. C. Benzel, D. K. Resnick and R. H. Rosenwasser, *Neurosurgery*, 2009, **64**, 214–215.
5 S. H. Im, D. H. Im, S. J. Park, Y. Jung, D. H. Kim and S. H. Kim, *Can. J. Cardiol.*, 2022, **126**, 100922.
6 P. Garg and L. Mauri, *Can. J. Cardiol.*, 2007, **22**, 565–571.
7 D. Stoeckel, A. Pelton and T. Duerig, *Eur. J. Radiol.*, 2004, **14**, 292–301.
8 S. H. Im, D. H. Im, S. J. Park, Y. Jung, D. H. Kim and S. H. Kim, *Prog. Mater. Sci.*, 2022, **126**, 100922.
9 F. Strickler, R. Richard, S. McFadden, J. Lindquist, M. C. Schwarz, R. Faust, G. J. Wilson and M. Boden, *J. Biomed. Mater. Res., Part A*, 2010, **92A**, 773–782.
10 P. A. Lemos and I. Bienert, *Expert Rev. Med. Devices*, 2013, **10**, 295–300.
11 S. M. Derkaoui, A. Labbe, P. Chevallier, S. Holvoet, C. Roques, T. Avramoglou, D. Mantovani and D. Letourneur, *Acta Biomater.*, 2012, **8**, 3509–3515.
12 L. M. Szott, C. A. Irvin, M. Trollsas, S. Hossainy and B. D. Ratner, *Biointerphases*, 2016, **11**, 29806.
13 K. V. Wolf, Z. Zong, J. Meng, A. Orana, N. Rahbar, K. M. Balss, G. Papandreou, C. A. Maryanoff and W. Soboyejo, *J. Biomed. Mater. Res., Part A*, 2008, **87A**, 272–281.
14 A. K. Mishra, J. Lim, J. Lee, S. Park, Y. Seo, H. Hwang and J. K. Kim, *Polymer*, 2021, **213**, 123329.
15 H. Guo, P. Chen, S. Tian, Y. Ma, Q. Li, C. Wen, J. Yang and L. Zhang, *Langmuir*, 2020, **36**, 14573–14581.
16 P. Raesian, M. S. Rad, E. Khodaverdi, V. S. Motamedshariaty and S. A. Mohajeri, *J. Drug Delivery Sci. Technol.*, 2021, **64**, 10259.

17 G. Wang, T. Zhang, S. Ahmad, J. Cheng and M. Guo, *Int. J. Adhes. Adhes.*, 2013, **41**, 198–205.
18 D. J. Kim, I. S. Park and M. H. Lee, *Ceram. Int.*, 2005, **31**, 577–581.
19 T. K. Sinha, J. H. Lim, H. R. Chothe, J. G. Kim, T. Nam, T. Lee and J. S. Oh, *J. Appl. Polym. Sci.*, 2022, **139**, e52396.
20 M. Contardi, D. Kossyvaki, P. Picone, M. Summa, X. Guo, J. A. Heredia Guerrero, D. Giacomazza, R. Carzino, L. Goldoni, G. Scoponi, F. Rancan, R. Bertorelli, M. Di Carlo, A. Athanassiou and I. S. Bayer, *Chem. Eng. J.*, 2021, **409**, 128144.
21 A. Isakova, C. Burton, D. J. Nowakowski and P. D. Topham, *Polym. Chem.*, 2017, **8**, 2796–2805.
22 Y. Ji, M. Hou, J. Zhang, T. Wang, C. Cao, H. Yang and X. Zhang, *Coatings*, 2022, **12**, 1074.
23 Z. Xi, Y. Xu, L. Zhu, Y. Wang and B. Zhu, *J. Membr. Sci.*, 2009, **327**, 244–253.
24 E. Amstad, A. U. Gehring, H. Fischer, V. V. Nagaiyanallur, G. Haehner, M. Textor and E. Reimhult, *J. Phys. Chem. C*, 2011, **115**, 683–691.
25 C. Zhang, L. Gong, L. Xiang, Y. Du, W. Hu, H. Zeng and Z. Xu, *ACS Appl. Mater. Interfaces*, 2017, **9**, 30943–30950.
26 Z. Ding, F. Fatollahi Fard, I. S. Kwon, P. C. Pistorius and C. J. Bettinger, *Adv. Eng. Mater.*, 2018, **20**, 1800621.
27 Y. Yan, W. Zhang, Y. Qiu, Z. Zhang, J. Zhu, Z. Cheng, W. Zhang and X. Zhu, *J. Polym. Sci., Polym. Chem.*, 2010, **48**, 5206–5214.
28 C. Zhang, L. Li, H. Cong and S. Zheng, *J. Polym. Sci., Polym. Chem.*, 2014, **52**, 952–962.
29 *E. DIN, 2409: 2013-06 Beschichtungsstoffe–Gitterschnittprüfung (ISO 2409: 2013)*, Beuth Verlag, Berlin, 2013.
30 S. Wang, Y. Zhang, Y. Qin, J. Lu and W. Liu, *Ceram. Int.*, 2023, **49**, 13405–13413.
31 L. Martín-Gomis, M. Fernández-García, J. L. de la Fuente, E. L. Madruga and M. L. Cerrada, *Macromol. Chem. Phys.*, 2003, **204**, 2007–2016.
32 F. R. Wurm and A. l. e. Gapin, *ACS Appl. Polym. Mater.*, 2022, **4**, 6863–6870.
33 Q. Zhang, X. Zhan, F. Chen, Y. Shi and Q. Wang, *J. Polym. Sci., Polym. Chem.*, 2007, **45**, 1585–1594.
34 H. Yang, Q. Wu, L. Wan and Z. Xu, *Chem. Commun.*, 2013, **49**, 10522–10524.
35 M. Wu, T. Wang, L. Mueller and F. A. Mueller, *Colloids Surf., A*, 2020, **603**, 125196.
36 J. Xu and S. Xu, *J. Appl. Polym. Sci.*, 2023, **140**, e53530.
37 N. T. Tran, D. P. Flanagan, J. A. Orlicki, J. L. Lenhart, K. L. Proctor and D. B. Knorr Jr, *Langmuir*, 2018, **34**, 1274–1286.
38 S. E. Kulkova, A. V. Bakulin, Q. M. Hu and R. Yang, *Phys. B*, 2013, **426**, 118–126.
39 W. Cheng, Y. Pan, T. Wu, C. Chou, C. Yeh and J. Ho, *Appl. Surf. Sci.*, 2019, **463**, 732–740.
40 S. A. Shabalovskaya, J. Anderegg, F. Laab, P. A. Thiel and G. Rondelli, *J. Biomed. Mater. Res., Part B*, 2003, **65B**, 193–203.
41 S. Wu, *J. Adhes.*, 1973, **5**, 39–55.
42 A. El Aferni, M. Guettari, M. Kamli, T. Tajouri and A. Ponton, *J. Mol. Struct.*, 2020, 1199.
43 R. Zhou, P. Ren, H. Yang and Z. Xu, *J. Membr. Sci.*, 2014, **466**, 18–25.
44 J. Jiang, L. Zhu, L. Zhu, H. Zhang, B. Zhu and Y. Xu, *ACS Appl. Mater. Interfaces*, 2013, **5**, 12895–12904.
45 N. Wang, Y. Zhang, J. Chen, J. Zhang and Q. Fang, *Prog. Org. Coat.*, 2017, **109**, 126–134.
46 C. Yang, C. B. Jacobs, M. D. Nguyen, M. Ganesana, A. G. Zestos, I. N. Ivanov, A. A. Puretzky, C. M. Rouleau, D. B. Geohegan and B. J. Venton, *Anal. Chem.*, 2016, **88**, 645–652.
47 M. Lazzari and M. A. López Quintela, *Adv. Mater.*, 2003, **15**, 1583–1594.
48 X. Liu, L. Lei, J. Hou, M. Tang, S. Guo, Z. Wang and K. Chen, *J. Mater. Sci.: Mater. Med.*, 2011, **22**, 327–337.
49 C. Park, E. Y. Kim, Y. T. Yoo and S. S. Im, *J. Appl. Polym. Sci.*, 2003, **90**, 2708–2714.
50 M. A. Frohoff-Hülsmann, A. Schmitz and B. C. Lippold, *Int. J. Pharm.*, 1999, **177**, 69–82.
51 S. Wang, Y. Zhang, Y. Qin, J. Lu and W. Liu, *Ceram. Int.*, 2023, **49**, 13405–13413.
52 P. Tian, D. Xu and X. Liu, *Colloids Surf., B*, 2016, **141**, 327–337.
53 M.-S. Hong, Y. Park, T. Kim, K. Kim and J.-G. Kim, *J. Mater.*, 2020, **6**, 158–166.
54 Y. Guo, S. Jia, L. Qiao, Y. Su, R. Gu, G. Li and J. Lian, *J. Alloys Compd.*, 2020, **817**, 152782.
55 T. Li, K. Ma and T. Zhang, *Prog. Org. Coat.*, 2022, **172**, 107084.